Spray Characteristics of a Fuel-water Internally Rapid Mixing Injector for Burner Combustion

Y. Nada[1*], Y. Kidoguchi[1], S. Yoshimura[1], K. Onoda[1], D. Asao[1], A. S. M. Arshad[2]
[1]Department of Energy System, The University of Tokushima, Japan
[2]Vehicle System Engineering Research Group, Universiti Teknologi Malaysia, Malaysia

Abstract

The fuel-water internally rapid mixing type of injector has been developed to reduce NOx and soot emissions from combustion furnaces operating under high-load conditions. The injector allows spray injection of water emulsified fuel originating from base fuel and water without any surfactants. The aim of present study is to elucidate the mechanism of emulsification occurring in the injector and the atomization characteristics of the injector. We measured the sizes of fuel droplets discharged from the injector by means of a high-speed shadowgraph method combined with image processing. Soybean oil was used as the base fuel. The flow patterns of the fuel and water in a transparent mixing chamber of the injector were also visualized. In addition, we investigated the inner structure of the large droplets sampled by an immersion droplet sampling method. The base fuel, water and air are separately introduced into the injector. In the mixing chamber of the injector, fuel and water are blown by swirling air, and then impinge on the inner wall of the chamber. The base fuel is emulsified through the mixing of fuel with water resulting from the impingement. The emulsified fuel moves to injection holes along the inner wall, and is finally discharged through the injection holes with atomizing air. The probability profiles of droplet size exhibit that the existence probabilities of coarse droplets with diameters greater than approximately 35 μm are increased when the fuel is emulsified. Although the emulsification deteriorates the atomization capability of the injector, the secondary atomization including the micro-explosion occurring in combustion furnaces would form fine droplets, and thus reducing the soot emission from the furnaces. The microscope observations revealed that the emulsified fuel filling in a large droplet sampled corresponds to W/O type.

Keywords: Fuel-water internally rapid mixing injector, Emulsification, Atomization, Combustion, Soot emission

Introduction

Over the last several decades, combustion researchers have made effort to reduce NOx and soot emissions from combustion furnaces. The combustion of emulsified fuel consisting of base fuel and water doped with surfactants, is a combustion technology able to simultaneously reduce the emissions [1]. When water emulsified fuel is injected into hot gases, the flash evaporation of the water dispersed in the fuel droplets causes the secondary atomization, namely micro-explosion [2-4] and puffing [4, 5], generating a large number of fine droplets [6], and increasing the combustion efficiency under conditions of optimum water contents [7, 8]. The soot emission from the emulsion combustion is mainly reduced by the enhanced mixing of fuel vapor with combustion air resulting from the flash evaporation [7, 9, 10]. Furthermore, OH radical originating from water dispersed in emulsified fuel oxidizes both soot and its precursors, leading to the soot reduction [10, 11]. The introduction of water into the flame via emulsified fuel injection also reduces the NOx emission [12], which is due to the pure dilution effect [13] and the chemical dilution effect associated with H_2O [14].

Our research group has developed a fuel-water internally rapid mixing injector which has some advantages regarding fuel emulsifications [15]. Base fuel, water, and atomizing air are separately introduced into the injector, and then the base fuel is emulsified with the water in the mixing chamber of the injector. Because the injector allows the emulsification without surfactants, the other emulsification equipment as well as surfactant is not required. Kajitani and Sawa [16] reported the aging deterioration of emulsified fuel, that is, increase in the Sauter mean diameter of water droplets dispersed in base fuel due to its coalescence. The deterioration increases the viscosity of the emulsified fuel, which probably degrades the NOx and soot emissions. In contrast, the base fuel introduced into our injector is emulsified just before the injection into furnaces, and hence it is possible to supply flesh emulsified fuels into furnaces via our injector. In addition, the water content can be changed in response to combustion situation during furnace operation. Spadaccini and Pelmas [8] reported that the combustion efficiency has a peak value at an optimum water content of emulsified fuel, and the use of emulsified fuel with excessive water content destabilizes the flame. The adjustment of water content by our injector could contribute to stable operations of combustion furnaces.

In our previous study [15], it was demonstrated that the injector allows simultaneous reductions of NOx and soot emissions from furnaces fueled with gas oil and soybean oil. However, the characteristics of fuel spray discharged from the injector, including the droplet diameter and the inner structure of droplets, have not been elucidated. The aim of the present study is to clarify the spray characteristics of emulsified fuel discharged from the injector, as well as the effects of the water content of emulsified fuel on NOx and soot emissions under high-load conditions.

Experimental Setup

Figure 1 shows a schematic cross-sectional diagram of the fuel-water internally rapid mixing injector. The injector is composed of a body having some flow channels and a co-axial slit, swirler, and mixing chamber with injection holes. The length of the injector is 107 mm. The water is introduced into the mixing chamber through the central channel while the base fuel is through the co-axial slit. The atomizing air flows into the chamber through some channels and the swirler providing a rotational flow in the chamber. The fuel and water introduced are blown by the swirling air, and then the base fuel is emulsified by the mixing of the fuel with the water. The emulsified fuel is discharged through eight holes with a diameter of 1.0 mm, circularly arranged in the upper section of the chamber. The direction of each injection hole inclines by 45 degree to the vertical direction.

We evaluated Sauter mean diameter (SMD) of droplets in sprays discharged from the injector by using shadowgraph images. Figure 2 shows schematics of experimental apparatus consisting of a spray chamber, injector, nano spark photography unit [17], and digital camera. The spray chamber has a cuboid shape with a height of 190 mm, and a square cross section of 180 mm × 180 mm. The injector is installed at the top surface of the chamber obliquely downward by 45 degree, such that a single spray is discharged into the chamber vertically downward while the other sprays are into a separated room. The atomizing gas and emulsified fuel in the chamber are withdrawn by a vacuum pump. Commercially obtainable soybean oil was used as the base fuel, which was supplied by a pump at designated mass flow rates controlled by needle valves and a mass flow meter (Keyence, FD-SS02A). Nitrogen was used as the atomizing gas alternative to air for safety reasons, the flow rate of which was also controlled by a mass flow meter (SMC PFA 721) and a valve. The volume flow rate of water introduced was measured by a calibrated rotameter.

The chamber has two optical windows made of silicate glass on opposed lateral sides, through which the parallel light emitted by the light source is sent to spray in the chamber at a short duration of 30 ns. Shadowgraph images of sprays were captured by a digital camera (Nikon D7000) with a ISO speed of 100 and a spatial resolution of 4.1 μm/pixel. By using this system, static images of droplets moving with a high velocity of the order of 100 m/s were obtained. The luminous intensities of the images are represented by 16-bit data. The detail of image processing evaluating SMD values will be explained in the following section.

In order to investigate the mechanism of fuel emulsification occurring in the mixing chamber of the injector, we observed fuel and water streams in a transparent mixing chamber by using a high-speed camera (NAC, MEMRECAM GX-1) with a frame rate of 5000 fps. In addition, we investigated the inner structure of emulsified fuel droplets discharged from the injector. A small shallow dish with a depth of 4.6 mm was inserted into a spray stream at a downstream location from the injection hole by 143 mm. Some large droplets in the spray immerged into the pool of silicon oil in the dish. Within one minute after the end of the sampling, we began to observe the droplets in the pool with a digital microscope (Yashika, Mk-UMS1). During the sampling of droplets,

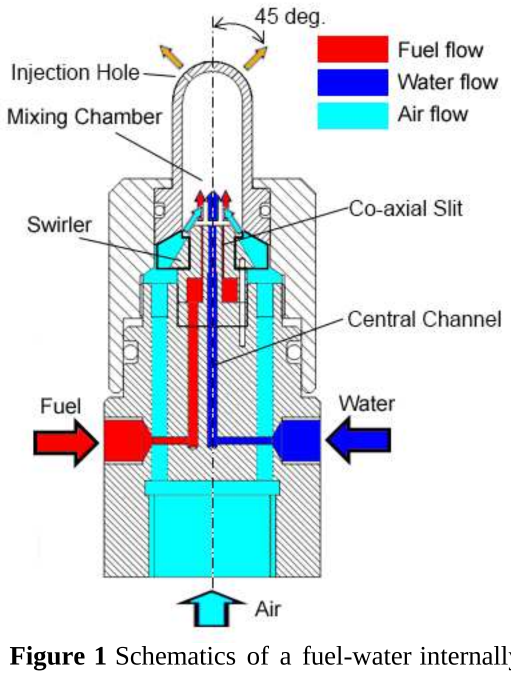

Figure 1 Schematics of a fuel-water internally rapid mixing injector.

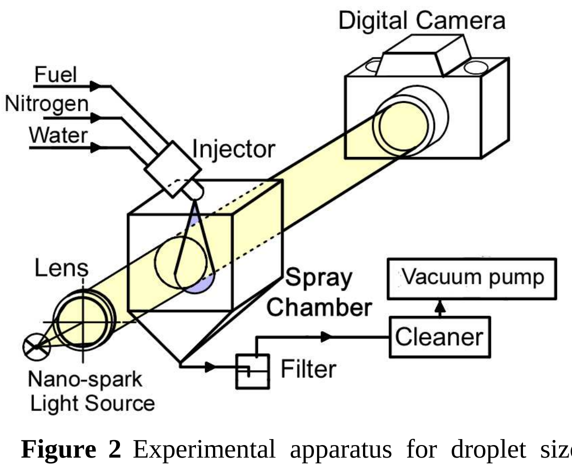

Figure 2 Experimental apparatus for droplet size measurements based on a shadowgraph method.

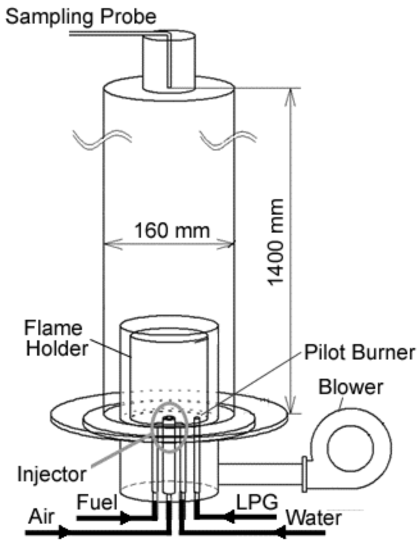

Figure 3 Experimental apparatus for NOx and soot measurements.

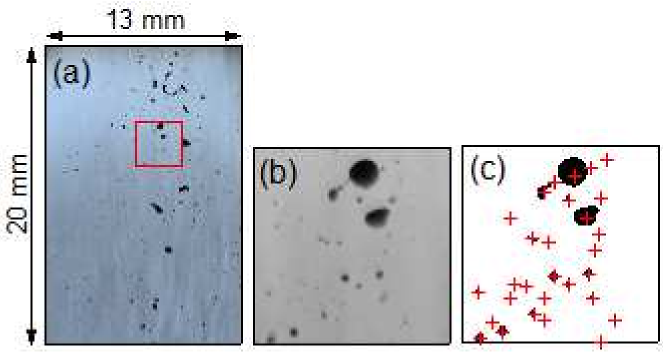

Figure 4 shadowgraph images. (a) shadowgraph image. (b) close-up image exhibiting the region indicated by red square in Fig 4 (a). (c) binarized image based on Fig. 4(b) in which red cross symbols denote the positions of luminosity centroid.

the water introduced into the injector was colored by red for easy identification of water in microscope images.

In our previous study [15], the effects of water introduction on NOx and soot emissions have been investigated. In this study, we newly measured the NOx and soot emissions from a laboratory-scale furnace to clarify the effects of water content on the emissions. Figure 3 shows schematics of experimental apparatus consisting of a combustion furnace, burner, and NOx and soot measurement system. Whereas a simple cylindrical tube with a length of 700 mm and an inner diameter of 160 mm was used as a furnace in the previous study [15], the furnace used in this study is extended to 1400 mm length, which is more than twice luminous flame length appearing in the furnace. As shown in Fig. 3, the furnace exit is contracted so as to ensure a uniform distribution of NOx concentration [18].

In the lower section of the cylindrical furnace a burner, which is composed of the fuel-water internally rapid mixing injector, a flame holder, and a pilot nozzle, is mounted. The detail of the burner has been already described in our previous paper [15]. We used a propane pilot flame at an ignition timing of the soybean oil flame. Secondary air is supplied from a blower into the furnace. The flue gases were sampled by a sampling probe inserted into the furnace through the exit. The inner diameter of the probe is 10 mm, and the flue gases were suctioned at a volume flow rate of 0.4 L/min by a vacuum pump. Since the lengths of flames were less than 700 mm, the temperatures of flue gases released from the exit were measured to be lower than 1000 K. Hence, NOx production through the Zel'dovich mechanism probably ceased until the flue gas reached to the exit. Therefore, the sampled gases in the probe were not cooled. The NOx concentration was measured by a gas analyzer (HORIBA, PG-240). Particulate matter (PM) existing in the flue gas was sampled by a filter inserted into the tube connecting the probe to the pump. The weight of sampled PM on the filter was measured by electronic scale (METTLER, AE240). After the soluble organic fraction (SOF) in the PM was eliminated by Soxhlet extractor, we measured the weight of the residue corresponding to dry soot. The weight of SOF component is defined as the difference between weights of PM and soot.

Image Processing for Evaluation of Droplet Diameter

We measured diameters of droplets in sprays by means of processing of images captured by shadowgraph method. Figure 4 (a) shows a shadowgraph image with a size of 20 mm × 13 mm, and the top of the image region is shifted by 10.5 mm downstream from the injection hole. Many droplets with various diameters can be found in this image, and some droplets seem to be in the breakup process. We evaluated a diameter of each droplet in the following manner [17, 19, 20].

1. Candidates for droplets are extracted from binarized images, and the position of the luminosity centroid of each candidate is determined.

2. The characteristic length of each droplet is evaluated on the distribution of luminous intensity gradient around the centroid.

3. Actual diameter of each droplet is obtained with a correlation between actual diameter and characteristic length.

Figure 4(b) shows a close-up image extracted from the image shown in Fig.4 (a). The image was binarized with a threshold value I_T defined as following equation.

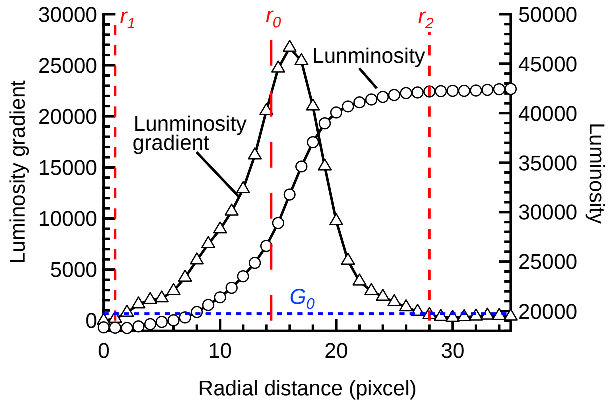

Figure 5 Radial distributions of luminosity and its gradient azimuthally averaged around the centroid.

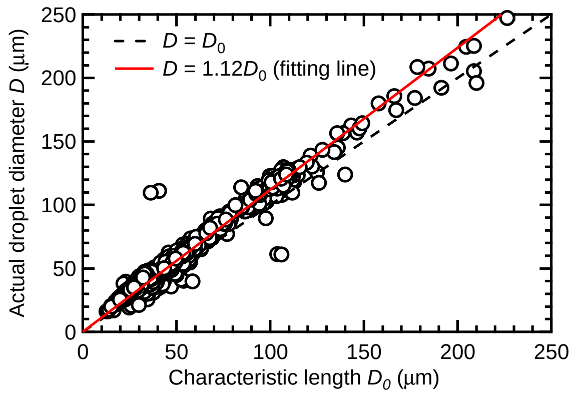

Figure 6 Correlation between characteristic length and actual diameter of ceramic ball.

$$I_T = \alpha\left(I_{mean} - I_{\min}\right) + I_{\min} \tag{1}$$

where I_{mean} and I_{min} are mean and minimum luminosities throughout the close-up region, respectively. Parameter α is set to 0.8. Figure 4 (c) shows the binarized image of the close-up region, in which black regions correspond to candidates for droplets, and the positions marked by cross symbol coincides with those of luminosity centroids of the candidates.

Figure 5 shows radial distributions of luminosity and its gradient azimuthally averaged around the centroid of a droplet candidate. Some obscure candidates corresponding to droplets existing off the focal surface were excluded on the basis of relation between minimum and maximum values of luminosity gradient. The characteristic length of the approved droplet r_0 is evaluated on following equation.

$$\int_{r1}^{r2} G(r)dr = \frac{1}{2}\int_{r1}^{r0} G(r)dr \tag{2}$$

In Equation (2), r denotes the radial distance from the centroid, and $G(r)$ represents the radial profile of luminosity gradient. r_1 and r_2 denote the radial distances of the positions where the value of luminosity gradient matches to the averaged gradient G_0 in a region outside the droplet. The inner position (= r_1) approximately coincides with the centroid. For almost droplets, the characteristic length is close to a distance from the centroid to the position where the gradient profile exhibits a peak. By employing above definition of the length, we can avoid under-estimation of diameter frequently occurring when the profile has several peaks.

Finally, the actual diameter of droplet is evaluated from the characteristic length. In order to obtain a correlation between actual droplet diameter and characteristic length, we prepared a glass plate on which approximately 1000 ceramic balls with various diameters, simulating fuel droplets, were scattered. The characteristic lengths of the ceramic balls were evaluated based on a shadowgraph image of the plate. On the other hand, the actual diameter of every ball was manually measured with a scale on enlarged images captured by a microscope. A linear correlation between characteristic length D_0 (= 2 r_0) and actual diameter D was obtained as shown in Fig. 6. The slope of the correlation line is 1.12, indicating that the actual diameter is 1.12 times of the characteristic length. The value of error introduced into the actual diameter is within 12 %.

Experimental Conditions

During the investigation of spray characteristics including SMD of droplets, the mass flow rate of base fuel M_f was maintained at 19.2 g/min, corresponding to an equivalence ratio of 0.9 under our combustion conditions. Nitrogen was selected as atomizing gas, the volume flow rate of which was also maintained at 56 NL/min. The mass flow rate of introduced water M_w was set to either zero or 10.5 g/min, such that the mass water content, defined as $Y_w = M_f / (M_f + M_w)$, was zero or 0.33. During the operation of the combustion furnace, the volume flow rates of atomizing air and secondary air were kept at 56 NL/min and 159 NL/min, respectively. The flow rate of atomizing air is equal to that of nitrogen used for the investigation of the spray characteristics. When NOx and soot emissions from the combustion furnace were measured, the volume flow rate of base fuel was varied from 19.2 g/min to 22.2 g/min, corresponding to the equivalence ratio ranging from 0.9 to 1.05.

Results and Discussion

Spray Characteristics of Internally Rapid Mixing Injector

Figure 7 shows existence probabilities of droplets with respect to diameter evaluated based on shadowgraph images. The number of sampled droplets extracted from the images is greater than 4700, and we confirmed that the probabilities shown in Fig. 7 have little correlation with the number of sampled droplets. When water is not introduced into the injector ($Y_w = 0$), the probability has a peak value at a diameter of 20 μm. Although the probability rapidly decreases with increasing diameter, several huge droplets with diameters greater than 100 μm can be found. As a result, the value of Sauter Mean Diameter (SMD) is increased up to 77 μm. When the water is introduced ($Y_w = 0.33$), the peak probability is lower than that for $Y_w = 0$ even though the diameter exhibiting the peak is close to that for $Y_w = 0$. Furthermore, the probabilities of droplets with diameters greater than 35 μm are higher than those for $Y_w = 0$. The SMD value is therefore increased up to 187 μm, which is greater than twice that for $Y_w = 0$. The increase in SMD value caused by the water introduction will be discussed later.

The formation of the huge droplets can be explained in terms of fuel streams in the mixing chamber. Figure 8 shows a series of successive images of the transparent mixing chamber when the base fuel is solely introduced. The location of the image region is indicated by a broken line in Fig. 8 (a). Red and blue arrows denote the flow directions of fuel and of atomizing air, respectively. We can observe the spiral stream of fuel with a shape of film attaching on the inner wall of the mixing chamber. The fuel film is formed as follows; the fuel introduced from the central channel is blown by the atomizing air with swirling motion, and then the blown fuel impinges on the inner wall of the chamber, forming the fuel film. As indicated by black arrows in Fig. 8 (b), there appear some dark regions in the transparent chamber, where the thickness of film is larger than that in other regions. The fuel film spirally moves downward along the inner wall. When the thick portion of the film reaches to the injection holes, a large amount of fuel is discharged from the holes with the atomizing air. Thus, the huge droplets responsible for the large SMD appear in the spray.

The SMD value measured in the present study would be greater than those of droplets discharged from conventional injectors. The existence of large droplets destabilizes the flame and increases pollutant emissions. For

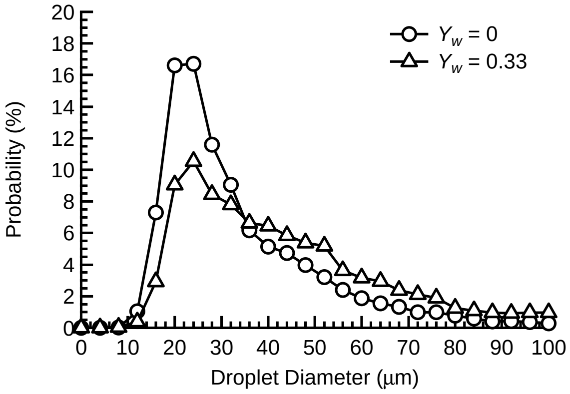

Figure 7 Probabilities of droplets with respect to diameter.

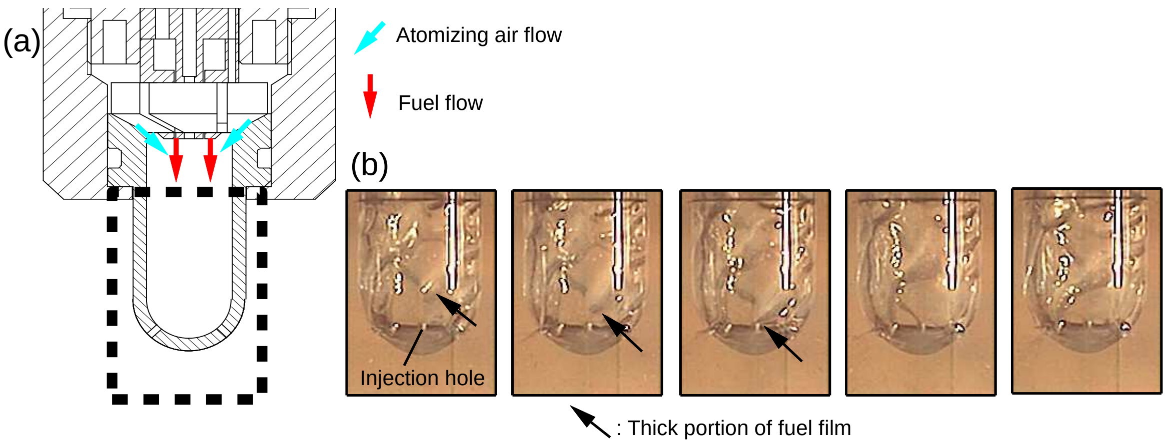

Figure 8 Images of the transparent mixing chamber when the base fuel is solely introduced. Figure 8 (a) shows cross-sectional schematic diagram of the injector, in which the location of the image region is indicated by a broken line. Figure 8(b) shows a series of successive images at time intervals of 18 ms.

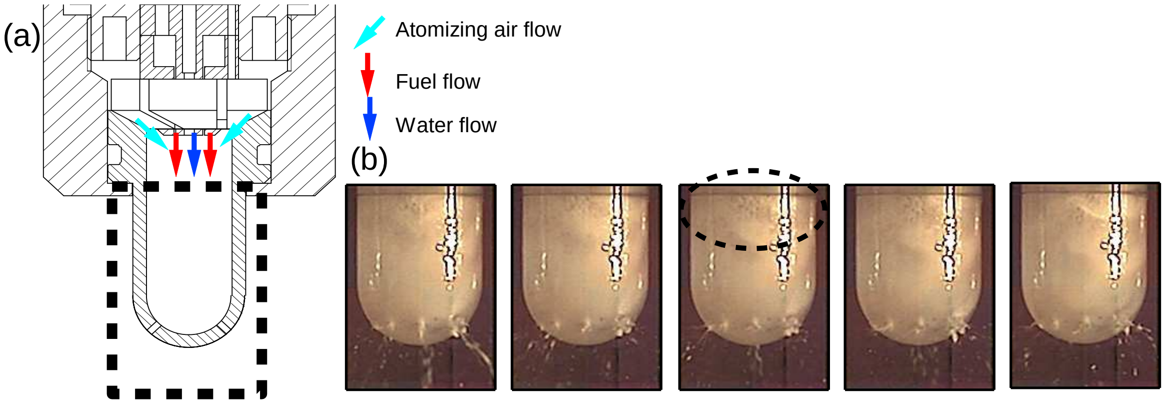

Figure 9 Successive images of the transparent mixing chamber at time intervals of 18 ms for Y_w = 0.33.

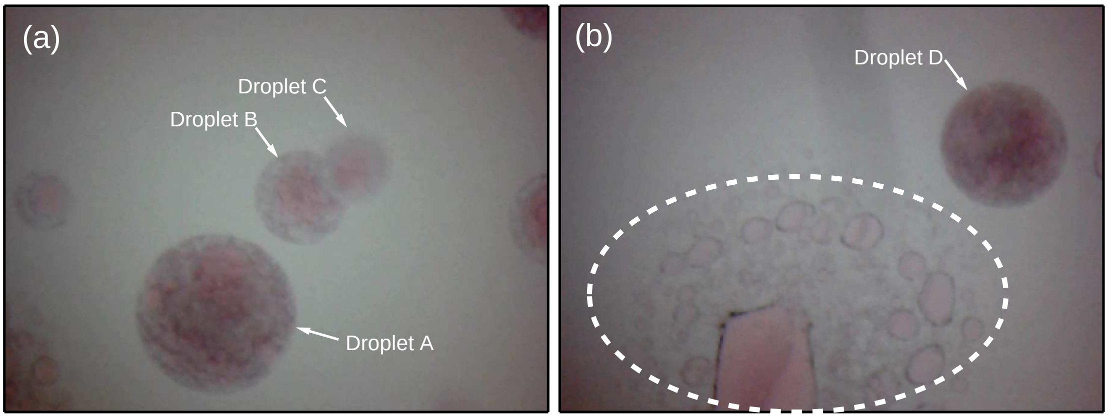

Figure 10 Microscope images of emulsified fuel droplet sampled by the immersion method. The water introduced into the injector is colored by red.

the purpose of the reduction of droplet diameter, we will try to uniform the film thickness by using a new type of swirler in our future works.

Figure 9 shows the successive images of the transparent mixing chamber for Y_w = 0.33. The mixing chamber seems to be filled with milky liquid since the film of emulsified fuel attaches on the inner wall. In the upper section of the mixing chamber, denoted by circle in the image, we can find transparent particles attaching on the inner wall, which are probably either pure fuel or water particles. It is evident from the images that the fuel mixes with the water through the impingement on the inner wall, resulting in the emulsification of the base fuel. The film of the emulsified fuel spirally moves to the injection holes as in the case of Y_w = 0. Since the emulsified fuel film is opaque, the spatial variation of film thickness cannot be observed in the series of the images. However, we were able to find the periodic fluctuation of discharge rate of emulsified fuel during experimental trials, which is exclusively due to the variation of film thickness.

Figure 10 shows the microscope images of droplets sampled by the immersion droplet sampling method. The size of the image region is 0.8 mm × 1.05 mm. As shown in Fig. 10 (a), droplets seem to contain some water particles colored by red, demonstrating that the emulsified fuel discharged from the injector is classified into the W/O type under our experimental conditions. In a previous study [21], the author reported that the viscosity of W/O type emulsified fuel increases with increasing water content, suggesting that the deterioration of atomization characteristics as shown in Fig. 7 is caused by the increase in the viscosity resulting from the emulsification.

Since the dish used for sampling is filled with silicon oil, the base fuel in the sampled droplets is solved in the oil. In a region enclosed by a broken circle shown in Fig. 10 (b), there appear a lot of water bubbles originating from the water particles dispersed in the emulsified fuel droplet. The biggest bubble observed here is formed through the coalescence among the particles in the sampling dish.

Suzuki et al. [4] investigated the effect of the water particle diameter on micro-explosion, and found that the increase in the water particle diameter relative to that of emulsified fuel droplet increases the occurrence probability of micro-explosion. Their results indicate that the diameter of dispersed water particle is a key element determining the combustion characteristics including the NOx and soot emissions. Unfortunately, we were not

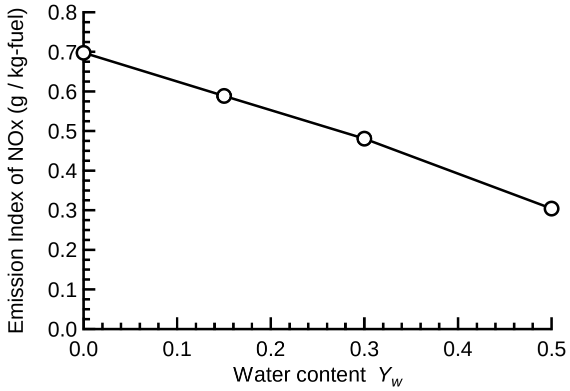

Figure 11 The effect of water content on NOx emission.

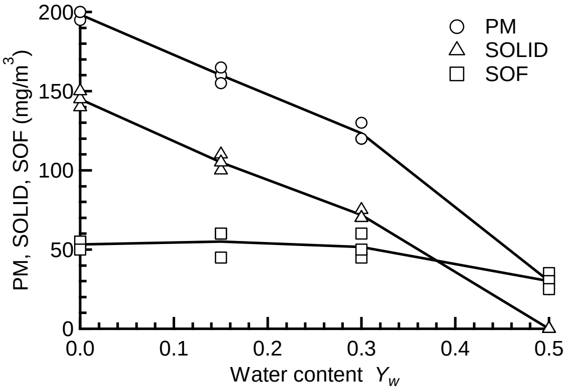

Figure 12 The effects of water content on PM, SOLID, and SOF emissions.

able to evaluate the diameter of dispersed water particle because the sampling method employed in the present study has a less accuracy for the evaluation. Almost droplets sampled by the immersion method have a diameter larger than SMD value, and hence, we have no images exhibiting the inner structure of fine droplets. Furthermore, the diameter of water particle increases with time through the coalescence among the particles because the base fuel is emulsified without any surfactant. Therefore, the diameters of water particles observed here might be much larger than those when existing in a spray. The investigation of inner structure of droplets including the size of dispersed water particles is also our future work.

NOx and Soot Emissions from Combustion Furnace with the Internally Rapid Mixing Injector

In this section, we will examine the emission characteristics of furnace combustion fueled with emulsified soybean oil discharged from our injector. Figure 11 shows emission index of NOx (EINOx) with respect to the water content Y_w measured during experimental trials at a global equivalence ratio of 0.9. EINOx is estimated according to a definition proposed by Turns and Myhr [22]. The value of EINOx decreases with increasing water content owing to the dilution effect [13] and the chemical effect [14].

Figure 12 shows the mass concentrations of PM, SOLID and SOF components measured at an equivalence ratio of 1.05. Since the measurements of the PM concentrations were made three times, this figure contains three plots at every experimental condition. Under the condition of an equivalence ratio less than unity, our measurement system was not able to collect measurable amount of PM. The PM concentration significantly decreases as the water content increases because the concentration of SOLID component corresponding to dry soot rapidly decreases. In contrast, the concentration of SOF component slowly decreases, such that PM released from the furnace operating at a condition of $Y_w = 0.5$ mostly consists of SOF component.

Hayashi et al. [23] demonstrated that an increase in SMD of droplets promotes soot formation in laminar spray flames because of the enhanced diffusion flame. As shown in Fig. 7, the emulsification by means of the injector increases SMD of droplets in the spray, which would contribute to the soot formation. However, as shown in this figure, the PM emission is reduced exclusively owing to the secondary atomization and OH radical attack. The simultaneous reductions of NOx and soot emissions indicate the excellent performance of our injector for the reduction of the emissions from furnaces operating at high load conditions.

Summary and Conclusions

In the present study, we investigated the characteristics of spray discharged from fuel-water internally rapid mixing injector being developed in our research group. The diameter of droplet in the spray was measured by shadowgraph method combined with the image processing. The mixing process occurring in the mixing chamber of the injector was investigated by using the high-speed camera and transparent mixing chamber. Furthermore, we observed the inner structure of emulsified fuel droplet sampled by immersion droplet sampling method, and finally examined the effects of the emulsification through the injector on the reductions of NOx and soot emissions.

The base fuel and water separately introduced into the injector are mixed with one another in the mixing chamber through the impingement of fuel and water on the inner wall, resulting in the emulsification of base fuel. The emulsified fuel discharged from the injector is W/O type such that the droplets in the discharged spray contain some water particles. The Sauter mean diameter of the droplet when water is introduced into the injector is much greater than that when base fuel is solely introduced, because of the increase in the viscosity of the emulsified fuel. The NOx and soot emissions are simultaneously reduced by the emulsification through the injector even though the mean droplet diameter of emulsified fuel increases. The soot reduction is due to the secondary atomization and OH radial attack to the soot.

References

[1] Kadota, T., and Yamasaki, H., *Progress in Energy and Combustion Science* 28: 385–404 (2002).
[2] Segawa, D., Yamasaki, H., Kadota, T., Tanaka, H., Enomoto, H., and Tsue, M., *Proceedings of the Combustion Institute* 28: 985–990 (2000).
[3] Yamasaki, H., Tsue, M., and Kadota, T., *JSME International Journal, Series B* 36: 677-681 (1993).
[4] Suzuki, Y., Harada, T., Watanabe, H., Shoji, M., Matsushita, Y., Aoki, H., and Miura, T., *Proceedings of the Combustion Institute* 33: 2063-2070 (2011).
[5] Wang, C. H., and Law, C. K., *Combustion and Flame* 59: 53-62 (1985).
[6] Mattiello, M., Cosmai, L., Pistone, L., Beretta, F., and Massoli, P., *Proceedings of the Combustion Institute* 24: 1573-1578 (1992).
[7] Nazha, M. A. A., and Crookes, R. J., *Proceedings of the Combustion Institute* 20: 2001-2010 (1984).
[8] Spadaccini, L. J., and Pelmas, R., *Evaporation- combustion of fuels*: 232-244.
[9] Tsue, M., Segawa, D., and Kadota, T., *Proceedings of the Combustion Institute* 26: 1251-1258 (1996).
[10] Kozinski, J. A., *Combustion and Flame* 96: 249-260 (1994).
[11] Rao, V. K., and Bardon, M. F., *Combustion and Flame* 55: 73-78 (1984).
[12] Mizutani, Y., and Taki, A., *Transaction of the JSME* 47: 2379-2385 (1981) (in Japanese).
[13] Liu, F., Guo, H., Smallwood, G. J., and Gülder, Ö. L., *Combustion and Flame* 125: 778-787 (2001).
[14] Shoji, M., Yamamoto, T., Tanno, S., Aoki, H., and Miura, T., *Energy* 30: 337-345 (2005).
[15] Yatsufusa, T., Kidoguchi, Y., and Nakagawa, D., *Journal of Energy and Power Engineering* 8: 11-19 (2014).
[16] Kajitani, S., and Sawa, N., *Transaction of the JSME* 56: 3542-3547 (1990) (in Japanese).
[17] Adam, A., Inukai, N., Kidoguchi, Y., Miwa, K., and Miyashiro, S., *SAE Technical Paper*, 2007-01-1893.
[18] Noda, S., Inohae, J., and Saldi, Z. S., *Proceedings of the Combustion Institute* 31: 1625-1632 (2007).
[19] Nawi, M. A. M., Kidoguchi, Y., Nakagiri, M., Uwa, N., Nada, Y., and Miyashiro, S., *SAE Technical Paper*, 2014-32-0125.
[20] Yatsufusa, T., Kidoguchi, Y., Adam, A., and Gomi, T., *Atomization: Journal of the ILASS-Japan* 18: 88-95 (2009) (in Japanese).
[21] Ishida, H., *Research Reports of Nagaoka National College of Technology* 48: 13-18 (2012).
[22] Turns, S. R. and Myhr, F. H., *Combustion and Flame* 87: 319-335 (1991).
[23] Hayashi, J., Watanabe, H., Kurose, R., and Akamatsu, F., *Combustion and Flame* 158: 2559-2568 (2011).